

**Repository of the Max Delbrück Center for Molecular Medicine (MDC)
in the Helmholtz Association**

<https://edoc.mdc-berlin.de/19055/>

Phosphodiesterase 3A and arterial hypertension

Ercu M., Markó L., Schächterle C., Tsvetkov D., Cui Y., Maghsodi S., Bartolomaeus T.U.P., Maass P.G., Zühlke K., Gregersen N., Hübner N., Hodge R., Mühl A., Pohl B., Molé-Illas R., Geelhaar A., Walter S., Napieczynska H., Schelenz S., Taube M., Heuser A., Anistan Y.M., Qadri F., Todiras M., Plehm R., Popova E., Langanki R., Eichhorst J., Lehmann M., Wiesner B., Russwurm M., Forslund S.K., Kamer I., Müller D.N., Gollasch M., Aydin A., Bähring S., Bader M., Luft F.C., Klussmann E.

This is a copy of the accepted manuscript, as originally published online ahead of print by the American Heart Association. The original article has been published in final edited form in:

Circulation
2020 JUL 14 ; 142(2): 133-149
2020 JUN 11 (first published online: final publication)
DOI: [10.1161/CIRCULATIONAHA.119.043061](https://doi.org/10.1161/CIRCULATIONAHA.119.043061)

Publisher: [American Heart Association | Lippincott Williams & Wilkins](#)

Copyright © 2020 American Heart Association, Inc.

Phosphodiesterase 3A and Arterial Hypertension

Running Title: *Ercu & Markó, et al.; Phosphodiesterase 3A*

Maria Ercu & Lajos Markó, et al.

The full author list is available on page 23.

Addresses for Correspondence:

Friedrich C. Luft, MD
Experimental and Clinical Research Center
(ECRC)
Lindenbergerweg 80
13125 Berlin, Germany
Tel.: +49-30-4505-40249
Email: Friedrich.Luft@charite.de

Enno Klussmann, PhD
Max-Delbrück-Center for Molecular Medi-
cine (MDC) in the Helmholtz Association
Robert Rössle-Strasse 10
13125 Berlin, Germany
Tel. +49-30-9406-2596
Email: enno.klussmann@mdc-berlin.de

Abstract

Background: High blood pressure is the primary risk factor for cardiovascular death worldwide. Autosomal-dominant hypertension with brachydactyly (HTNB) clinically resembles salt-resistant essential hypertension and causes death by stroke before age 50 years. Recently, we implicated the gene encoding phosphodiesterase 3A (*PDE3A*); however, *in vivo* modeling of the genetic defect and thus showing an involvement of mutant *PDE3A* is lacking.

Methods: We used genetic mapping, sequencing, transgenic technology, CRISPR-Cas9 gene editing, immunoblotting, and fluorescence resonance energy transfer (FRET). We identified new patients, performed extensive animal phenotyping, and explored new signaling pathways.

Results: We describe a novel mutation within a 15 bp region of the *PDE3A* gene and define this segment as mutational hotspot in HTNB. The mutations cause an increase in enzyme activity. A CRISPR/Cas9-generated rat model, with a 9 bp deletion within the hotspot analogous to a human deletion, recapitulates HTNB. In mice, mutant transgenic *PDE3A* overexpression in smooth muscle cells confirmed that mutant *PDE3A* causes hypertension. The mutant *PDE3A* enzymes display consistent changes in their phosphorylation and an increased interaction with the 14-3-3 θ adaptor protein. This aberrant signaling is associated with an increase in vascular smooth muscle cell proliferation and changes in vessel morphology and function.

Conclusions: The mutated *PDE3A* gene drives mechanisms that increase peripheral vascular resistance causing hypertension. We present two new animal models that will serve to elucidate the underlying mechanisms further. Our findings could facilitate the search for new antihypertensive treatments.

Key Words: Hypertension; Genetics; Blood pressure regulation; Phosphodiesterase

Non-standard Abbreviations and Acronyms

HTNB, hypertension with brachydactyly

DEL, functional deletion

Clinical Perspective

What is new?

- This study provides evidence that mutant, overactive phosphodiesterase 3A causes hypertension in a new family with HTNB and in novel rodent models.
- The mechanism underlying the hypertension resides inside vascular smooth muscle.

What are the clinical implications?

- The findings direct attention to new potential therapeutic targets for lowering blood pressure, namely phosphodiesterase 3A signaling and protein-protein interactions within the vascular wall.

Introduction

Hypertension is the primary cardiovascular-disease risk factor.¹ Mendelian genetics has elucidated blood-pressure-elevating mechanisms.² We reported earlier that hypertension with brachydactyly type E (HTNB) is an autosomal dominant, non-salt-sensitive, form of hypertension.³ If untreated, patients die of stroke by the age 50 years. We found mutations in seven independent HTNB families within a 15 base pair (bp) region of the phosphodiesterase (*PDE*)3A gene (Figure 1).^{4,5} Since our reports, other families have been described, suggesting that a mutant PDE3A enzyme causes HTNB. However, *in vivo* modeling of the genetic defect to test this hypothesis was lacking.

PDEs comprise 11 enzyme families degrading cyclic adenosine monophosphate (cAMP) and cyclic guanosine monophosphate (cGMP). Some enzymes degrade both, cAMP and cGMP, such as PDE3A.⁶ PDE3A exists in three isoforms that are derived from a single gene and the same transcript.⁷ They all contain the same catalytic domain and are similar in activity and inhibitor sensitivity but differ at their N terminus (Figure 1). PDE3A1 is the major form in human heart, PDE3A2 is the dominant isoform in human vascular smooth muscle cells (VSMC), and PDE3A3 is predominantly expressed in placenta.⁷

The HTNB mutations cause amino acid substitutions in PDE3A1 and A2 enzymes N-terminally of the catalytic domain. This region is not present in PDE3A3 (Figure 1). The mutant enzymes are hyperactive and two serine residues, S428 and S438, are aberrantly phosphorylated by protein kinase A (PKA) and/or protein kinase C (PKC); alanine substitutions decreased PDE3A activity.⁴ We now report an additional family with HTNB, whose mutation lies within the 15 bp regulatory region of the *PDE3A* gene. More importantly, we present two novel animal models

that support the hypothesis that mutant PDE3A causes HTNB and increases peripheral vascular resistance.

Methods

All supporting data are available within the article and its online Supplemental Material that also includes further details. The analytic methods will be made available to other researchers for purposes of reproducing the results in their own laboratories upon request.

Analysis of patient mutations

The Ethical Committee of the Charité and the local Internal Review Boards approved the studies. Written informed consent, including consent for publication of results with images, was obtained from all participants. Patient DNA was analyzed with conventional Sanger sequencing.⁴

Rat Model

State of Berlin authorities approved the rat studies according to American Physiological Society guidelines (license no. G 0435/17). The rat model (Figure 2) was generated by pronuclear microinjection of Sprague-Dawley rat zygotes with a mixture of 25 ng/μl Cas9 mRNA, 30 ng/μl Cas9 protein (both from IDT, Skokie, IL, USA) and 12.5 ng/μl of *in vitro*-transcribed gRNA with the sequence 5'-AGGCAGTCCTGTGGCAGAGG (IDT, Skokie, IL, USA) to target the region in the rat *Pde3a* gene homologous to the human T445N mutation. The injected zygotes were cultured to the two-cell stage and transferred into foster mothers according to established methods.⁸ The offspring were genotyped by PCR with primers flanking the gRNA target region (PDE3a5, 5'-CTTCCGCTCCTTGCTTTACC; PDE3a3, 5'-GTAAGTCCTCTGAGGAGACC) and sequencing of the PCR fragment.

Animal phenotyping and interventions

Male rats (500-600 g, ca. 9 months) were used in all experiments. They were anesthetized with isoflurane (CuraMed Pharma GmbH, Karlsruhe, Germany). The pressure-sensing HD-S10 device (Data Science International) was placed into the abdominal aorta, and the transmitters into a subcutaneous pocket along the right flank. Blood pressure and heart rate was recorded using the DATAQUEST software (A.R.T. 2.1, Data Sciences International).

Telemetry measurements following at least one week after recovery from implantation were recorded continuously at 5 min intervals for 10 s continuously day and night in freely moving animals. The data were analyzed using mixed-effects modeling. Animal identity and time point within a day were included as random effects. Genotype, animal sex and day/night status at time of measurement were included as fixed effects, using the R lme4 package. The scopes of effects were obtained from the model parameters (slope and intercept parameters). The significance of each factor was assessed by comparing each linear model to a simpler model omitting the genotype as a predictor; here, likelihood ratio tests were performed as implemented in the lmerTest R package. Data were visualized using loess regressions from the ggplot2 R package.

Left front paws were scanned *ex vivo* in a micro-computer tomography (CT) scanner (SkyScan 1276, Bruker). The vendor's software was used for image acquisition (v.1.0.8). For imaging PICA loops, rats were anesthetized with isoflurane (4-5 %) and intracardially perfused with approximately 50 mL of warm heparinized normal saline solution, followed by 8 mL of Microfil (Flow Tech, Inc., Carver, Massachusetts, USA) solution. The agent was allowed to harden (90 min), the brain was removed and kept in 4 % paraformaldehyde solution overnight. μ CT was performed using a Skyscan 1276 scanner.

Echocardiography was performed (detector MS-250), and data were visualized and analyzed *via* the VEVO 2100 high-resolution imaging system (Visualsonics Fujifilm, VisualSonics, Toronto, Ca).

Rats were treated with BAY 41-8543 (Cayman Chemical) in a formulation of Transcutol/Cremophor-EL/water (10 %:20 %:70 %) per gavage to reach a dose of 3 mg/kg as described.⁹

Plasma and urine samples were measured at the Animal Phenotyping Platform of the Max Delbrück Center for Molecular Medicine (Berlin, Germany) using an AU480 Beckman Coulter chemistry analyzer. Circulating angiotensin levels and aldosterone and renin concentrations were measured by Attoquant Diagnostics GmbH (Vienna, Austria) as described earlier.¹⁰

Vascular isometric contractions and pressure myography

Rat aorta were removed immediately after sacrificing the animals and dissected into 5 mm rings. In a Mulvany Small Vessel Myograph (DMT 610 M; Danish Myo Technology, Denmark), the rings were placed under a tension equivalent to that generated at 0.9 times the diameter of the vessel at 100 mmHg by stepwise distending vessels using the LabChart DMT Normalization module. This normalization defined the passive diameter of the vessel at 100 mmHg. The basal tone of aortic rings was continuously monitored and adjusted to 1 g using the Organ Bath System (AD Instruments Ltd. Spechbach, Germany). The software Chart5 (AD Instruments) was used for data acquisition and display. After 60 min equilibration, vessels were pre-contracted with phenylephrine (PE) until a stable resting tension was acquired and pharmacological agents were added into the bath. Tension is expressed as a percentage of the steady-state tension (100 %) obtained with PE.

Pressure myography was performed as previously described.¹¹ Third-order mesenteric arteries were dissected from the rats and mounted on glass cannula. They were perfused continuously with physiological saline solution (PSS) containing (mM): 119 NaCl, 4.7 KCl, 25 NaHCO₃, 1.2 KH₂PO₄, 1.6 CaCl₂, 1.2 MgSO₄, and 11.1 glucose pH, 7.4, under 95% O₂-5% CO₂ at 37°C. The intravascular pressure was incrementally elevated from 20 to 100 mmHg using a pressure servo control system (Living System Instrumentation, Burlington, VT). We measured the vascular inner diameter with a video microscope (Nikon Diaphot, Düsseldorf, Germany) connected to a personal computer for data acquisition and analysis (HaSoTec, Rostock, Germany). Arteries were equilibrated at 15 mmHg for 60 minutes and contractile responsiveness assessed by applying 60 mM KCl.

Histological staining and cAMP detection

Second-order rat mesenteric arteries were removed immediately after sacrificing the animals under isoflurane anesthesia. The vessels were dissected into 4 mm rings and cAMP was measured using radioimmunoassays (RIA) as described.¹² Alternatively, the second-order arteries were stained with Hematoxylin-Eosin (Sigma, Germany). Using an inverted microscope (Keyence BZ-9000, Germany) and imaging with Keyence BZ-9000 Analysis Software System, media-to-lumen area measurements were performed. Data were quantified using Excel and GraphPad Prism.

Cell proliferation assays

Thoracic aorta was obtained from male SD rats and VSMC were isolated as previously described.¹³ Primary VSMCs of passages 5–9 were counted using a sceptor device (Millipore Sceptor Handheld automated cell counter, # PHCC00000).

Plasmids and antibodies

The vector encoding Flag-tagged PDE3A2³ was modified by site-directed mutagenesis to encode the PDE3A2-Δ3aa deletion. In addition, mCherry-tagged PDE3A2-T445N, PDE3A2-G449S, and PDE3A2-Δ3aa were generated. The plasmid pcDNA3-ICUE3 was purchased from Addgene (Plasmid #61622). The following vectors were used as controls for the FRET measurements: pcDNA3-CFP (Plasmid #13030), mVenus-C1 (Plasmid #27794) and CFP-YFP tandem construct (kindly provide by Dr. C. Rutz, Leibniz-Forschungsinstitut für Molekulare Pharmakologie (FMP) Berlin, Germany).

Rats were immunized with peptides RR(pS428)LPPGLLRRVSSTW and RSLPPGLLRRV(pS438)STW to generate antibodies against phosphoserine 428 and 438 (Eurogentec). The following antibodies were purchased: anti-phospho-S312 antibody (University of Dundee), PDE3A (Bethyl; A302-740A), GAPDH (Cell Signaling; 14C10), the “anti-DDDDK tag coupled to Hrp” (Flag-Hrp) antibody (GeneTex; 77454), 14-3-3θ (Santa Cruz; sc69720), smooth muscle actin (Cell Signaling; 14968), secondary antibodies anti-rabbit (#711-036-152), anti-mouse (#715-035-151) and anti-rat (#712-035-153) were from Jackson Immuno Research, and anti-sheep from Invitrogen (#61-8620).

Fluorescence resonance energy transfer (FRET) measurements

HEK293 cells (3×10^5) were seeded on glass coverslips in 6-well plates and transfected to transiently express the sensor ICUE3¹⁴ alone, to co-express ICUE3 and PDE3A2-mCherry constructs, or the controls, cyan fluorescent protein (CFP) and Venus either alone or together, or a CFP-yellow fluorescent protein (YFP) tandem construct. FRET imaging was performed on an inverted confocal laser scanning microscope (CLSM510-META-NLO; Carl Zeiss) equipped with a Plan-

Neofluar 40x/1,3 (Oil). CFP, excitation at 810 nm (Chameleon™ diode-pumped laser; Coherent), emission 430 to 505 nm; Venus or YFP, excitation at 514 nm with an argon laser, emission 520 to 560 nm; mCherry, excitation at 543 nm, a LP 560 nm long-pass emission filter for fluorescence detection; FRET, excitation at 810 nm, emission at 430 to 655 nm. To calculate the FRET-based fluorescence, a γ -stack with a linear spectral unmixing mode was used in order to correct any YFP fluorescence cross-talk into the FRET channel (523-532 nm). The γ -stack is an integral part of the confocal laser system software. YFP correction was carried out to correct for direct excitation of the acceptor during donor excitation.

The effect of treatments with pharmacological agents on cAMP levels was expressed by changes in the FRET ratio, which is calculated by dividing the acceptor emission (Venus, 532 nm) by the donor emission (CFP, 458 nm). Δ FRET (%) was calculated by subtracting the FRET ratio obtained upon stimulation from the FRET ratio of the control condition and normalization of the value to the FRET ratio of the control condition and multiplying by 100 to yield percentage.

Biochemical and molecular biological methods

Immunoprecipitation, Western blotting and qRT-PCR were carried out as previously described.^{4,}

15, 16

Statistics

Statistically significant differences were determined by one-way and two-way ANOVA and Bonferroni multi-comparison, Student's t-test or log-rank (Mantel-Cox) test. $p < 0.05$ was accepted as significant. Telemetry data were analyzed by likelihood ratio comparisons of nested

mixed effects models assessing whether genotype adds predictive power to a model already containing animal ID and time as random effects, and day-night stage as fixed effect, using the R *lme4* and *lmerTest* packages.

Results

A mutation in a hotspot region of the *PDE3A* gene causes HTNB

A woman aged 54 years (Figure 3; I/2; Supplemental Material, Table I in the Supplement) with a 17-year history of hypertension was admitted to hospital with blood pressure of 190/100 mmHg. The short fingers and toes are documented in the photograph and the roentgenogram (Figure 3). Our analysis of the patient and her 23-year old daughter revealed a mutation in exon 4 of the *PDE3A* gene causing a G449S (glycine-to-serine) substitution in the enzyme. Earlier, others and we reported a G449D substitution.^{5, 17} In addition, a S446P substitution¹⁸ and a 3 bp T445del was discovered in HTNB families.¹⁹ Thus, all HTNB mutations affect a region of 15 bp in exon 4 of the *PDE3A* gene encoding a 5 amino acid segment (amino acids 445-449) N-terminally of the catalytic domain (Figure 1).

A *Pde3a* mutation recapitulates HTNB in a rat model

To prove that mutations in the mutational hotspot of the *PDE3A* gene cause HTNB, we generated animal models. The rat model exhibits a 9 bp deletion within the hotspot that leads to the loss of three amino acids (aa 441-443 analogous to human PDE3A aa 444-446; Figure 2). The Δ 3aa deletion corresponds to the human deletion, T445del.¹⁹ Since HTNB is autosomal dominant, the heterozygous condition matches the situation in the patients. We also generated a rat strain with a frame-shift mutation (Δ 20 bp) that produces a truncated protein and, when homozygous, a functional deletion (DEL) of PDE3A.

In aorta of the WT and the heterozygous (HET) $\Delta 3aa$ rats, two PDE3A isoforms were detected, corresponding in size to PDE3A1 and A2. The expression of both isoforms was reduced in the $\Delta 3aa$ HET rats, which may be due to altered phosphorylation and protein-protein interactions of the mutant enzyme (see below) and thus altered detection by our antibody. Apparently, the remaining wild-type allele encoding the PDE3A isoforms did not compensate the reduction in expression. Both proteins were undetectable in the homozygous functional DEL animals (Figure 4A). MicroCT imaging of the left front paws confirmed short fingers typical for HTNB, metacarpal bone III was significantly shorter (Figure 4B) and its volume was significantly smaller (Figure IA in the Supplement) in the $\Delta 3aa$ HET rats than the WT. Also, the $\Delta 3aa$ HET animals were around 20 % lighter than the WT rats (Figure IB in the Supplement).

Radio-telemetry was performed at age >9 months. The data show mean systolic (SBP) and diastolic (DBP) blood pressure values of 148/105 mmHg in $\Delta 3aa$ HET rats, while the functional DEL rats had SBP and DBP values of 115/84 mmHg. WT rats had SBP and DPB values at 125/88 mmHg. We have encountered no homozygous patients in our PDE3A families; however, we crossed the $\Delta 3aa$ HET rats to produce a homozygous $\Delta 3aa/\Delta 3aa$ strain (HOM). Their blood pressure was 155/120 mmHg (Figure 4C). The WT, the $\Delta 3aa$ HET and HOM rats had similar heart rates (WT, 297 beats per min; $\Delta 3aa$ HET, 293 beats per min; and $\Delta 3aa$ HOM, 294 beats per min) that were all lower than those of the PDE3A functional DEL animals (330 beats per min; for statistical analysis see Table II in the Supplement). The echocardiographic estimates of cardiac output, ejection fraction and further cardiac parameters in the $\Delta 3aa$ HET and HOM rats was not significantly altered compared to WT animals (Figure 4D, Figure IC in the Supplement). We described possible neurovascular aberrations in 15 HTNB patients. The patients all had left-side posterior inferior cerebellar artery (PICA) or vertebral artery loops.²⁰ MicroCT imaging of brain

vessels revealed that the $\Delta 3aa$ HET rats also exhibited PICA loops. Loops were not detected in any WT animal (Figure 4E).

The aortas of WT, $\Delta 3aa$ HET, and PDE3A functional DEL rats did not exhibit an increased size of the media (Figure ID in the Supplement). To test their function, aortic rings from the rats were pre-constricted with phenylephrine. Adenylyl cyclase stimulation with forskolin triggered about a 40 % reduced relaxation of rings from $\Delta 3aa$ HET rats (relatively resistant) and an increased relaxation of rings from PDE3A functional DEL rats compared to the WT controls (Figure 4F). In HTNB patients, an increased peripheral resistance and hyperplasia of peripheral arterial *Tunica media* are the only hypertension-relevant features. Similar to the human situation, the median to lumen ratio of second-order mesenteric arteries of the $\Delta 3aa$ HET rats was increased compared to the WT animals. In the functional DEL animals, the ratio was decreased compared to WT (Figure 4G). Moreover, due to the hyperactivity of the $\Delta 3aa$ PDE3A variant (see below) the cAMP values were lower in such vessels derived from $\Delta 3aa$ HET than in those from WT animals (Figure 4H).

Next, we pressurized third-order rat mesenteric arteries isolated from WT and $\Delta 3aa$ HET rats (Figure 4I). Myogenic tone was assessed over a range of intraluminal pressures between 20 and 100 mmHg. The myogenic tone of the vessels was similar at all pressures. However, the pressurized (100 mmHg) vessels from $\Delta 3aa$ HET rats showed weaker vasodilation in response to forskolin than those from WT animals. The diameter of vessel from the $\Delta 3aa$ HET rats changed by about 5 % compared to the 10 % change in the WT animals (Figure 4I). The data indicate that the basal myogenic tone is not affected by mutant PDE3A (see below) but that upon stimulation of the adenylyl cyclase/cAMP system hyperactivity of PDE3A (see below) limits the ability of small arteries to dilate. The data confirm our findings obtained by wire myography (Figure 4F).

We had previously observed that patient-derived stem cells differentiated into VSMC grew at a faster rate than those of unaffected family members.⁴ Similarly, the proliferation rate of VSMC from the $\Delta 3aa$ HET rats was increased compared to those of VSMC from WT or functional DEL animals. The cell number after 120 h in culture was 50 % higher than the number of WT cells (Figure 4J). As in mouse VSMC where *Pde3a* was deleted²¹, the VSMC from our PDE3A functional DEL rats grew at a similar rate as the those from the WT animals. Transient expression of the $\Delta 3aa$ PDE3A2 version in HEK293 cells also led to higher proliferation rates than expression of the WT (data not shown).

PDE3A is inhibited by cGMP.²² To stimulate cGMP synthesis in our WT and $\Delta 3aa$ HET rats, we treated the animals with a single-gavage dose (3 mg/kg) of a soluble guanylyl cyclase (sGC) stimulator, BAY 41-8543, as previously described.⁹ The compound is a derivative of the drug, riociguat, which is approved for the treatment of pulmonary hypertension in similar doses (maximal daily dose of 7.5 mg). HEK293 cells express sGC, and BAY 41-8543 raised the cGMP level and caused inhibition of WT PDE3A2 and apparently stronger of the $\Delta 3aa$ version (Figure IE in the Supplement, see below). Within three hours, BAY 41-8543 reduced the mean arterial blood pressure in the $\Delta 3aa$ HET stronger than in the WT rats, i.e. from 114 to 92 mmHg in the $\Delta 3aa$ HET rats and from 99 to 91 mmHg in the WT animals. The levels that were reached were similar (Figure 4K). The lower levels were stable for around 12 h; blood pressure reached original levels after around 24 h. A further single-gavage dose treatment of the same animals, 24 h after the initial administration had similar effects as the first treatment (Figure IF in the Supplement).

We also generated a conditional mouse model that expresses the T445N-encoding mutation as a human PDE3A2 transgene in smooth-muscle cells (Figure IIA in the Supplement). Hemizygous transgenic mice were used for the analysis (MyhCre⁺/PDE3A2-T445N⁺). As controls, littermate mice not expressing the transgene were used. Mice overexpressing wild-type PDE3A2 were not available. The transgenes were reduced in bodyweight and lived shorter than the control animals (Figure IIB). The reason for the smaller litter sizes and shorter survival rates of the mutants is unclear. The protein and human transgene *PDE3A2* mRNA were detected in bladder, aorta and first- and second-order mesenteric arteries of the mutant animals, but not in the controls. However, leaky expression of the transgene in skeletal muscle was observed. mRNA expression of the endogenous mouse *Pde3a* was detected in all tissues to similar degrees in transgenic and control animals (Figures IIC and D in the Supplement). The transgenic mice were hypertensive with SBP of about 126 mmHg, DBP of about 85 mmHg while controls were 115/84 mmHg, and their heart rate was decreased (Figure IIE in the Supplement). Blood pressure data of two mice, not included in the analysis because they did not survive the 10-day radio-telemetry observation, are documented in Figure IIF in the Supplement. One mouse had a blood pressure of 155/125 mmHg for 5 days before it died. Another mouse was fairly normotensive for 5 days and then developed a massive increase in blood pressure to 270/200 mmHg before it died. The media of aorta from the transgenes was not different from the control animals (Figure IIG in the Supplement). Mesenteric arteries from the transgene-expressing mice, pre-constricted with the adrenergic agent phenylephrine, reached around 25 % less dilation than the arteries from control animals in response to stimulation with forskolin (Figure IIH in the Supplement), suggesting an enhanced level of cAMP degradation. Thus, the mouse model underscores that hyperactive PDE3A2 in VSMC results in hypertension.

Serum and urine parameters in HTNB models are in the physiological range

We next evaluated serum and urine parameters in our animal models. All parameters (Table 1) were similar in WT and $\Delta 3aa$ HET rats. Chloride in urine, the fractional sodium (FENa) and chloride excretion (FECl) in the functional DEL rats were significantly greater than in WT animals. The reason for the differences is unknown. Serum and urine parameters of the transgenic mice were not different from the control animals (Table III in the Supplement). Furthermore, we found no proteinuria or perturbed renal function in the mutant animals. Albumin, creatinine, and urine/albumin creatinine ratios were no different, compared to WT animals (Table 1, Table III in the Supplement).

Angiotensin-II (Ang II) levels, angiotensinogen, aldosterone and plasma renin concentrations were also not significantly different between the control and mutant rats (Figure 5 and Table 1). The mRNA expression of the renal damage markers *Lcn2* and *Havcr1* was not altered in the $\Delta 3aa$ HET rats compared to WT; however, in the functional DEL rats *Lcn2* was upregulated (Figure IG in the Supplement). Similarly, in our transgenic mice, Ang II levels, angiotensinogen, aldosterone and plasma renin concentrations or *Lcn2* and *Havcr1* were not altered compared to control animals (Figures III and J in the Supplement, Table III in the Supplement). Thus, our $\Delta 3aa$ HET rat and the transgenic mouse models resemble our patients, who aside from stroke also had little evidence of target-organ damage, and hardly deviate from values observed in patients with essential hypertension.²³

Aberrant signaling of HTNB PDE3A2 mutants

To obtain insight into the molecular mechanisms underlying the HTNB phenotype, we measured the activity of our new mutant G449S and the $\Delta 3aa$ variants using fluorescence resonance energy transfer (FRET) in HEK293 cells. The cytosolic cAMP sensor, ICUE3,¹⁴ consists of a cAMP

binding domain of exchange protein directly activated by cAMP (Epac) flanked by cyan fluorescent protein (CFP) and Venus, a variant of yellow fluorescent protein (YFP). Upon cAMP binding, the sensor undergoes a conformational change that increases the distance between CFP and Venus and thereby decreases FRET (Figure IIIA in the Supplement). The sensor was co-expressed with WT or mutant (T445N, G449S, or Δ 3aa) PDE3A2-mCherry in HEK293 cells. The PDE3A2 versions were expressed at similar levels and were mainly located in the cytosol (Figure 6A). The emission intensity of the sensor was determined in the absence or presence of forskolin and the PDE3A inhibitor milrinone. Changes in FRET and thus activity of the PDE3A2 versions are shown as Δ FRET, which reflects the difference in emission intensity. An increase in Δ FRET indicates increased cAMP, consistent with decreased PDE3A activity. In cells expressing the T445N, G449S or the Δ 3aa mutant, forskolin led to a reduction in the Δ FRET compared to the WT, reflecting less cAMP in the mutant expressing cells than in WT expressing ones. The data indicate that mutations in the hot spot region of the *PDE3A* gene cause an increase in PDE3A2-mediated cAMP hydrolysis. The differences were abolished by the PDE3A inhibitor, cilostamide, indicating similar sensitivity of the WT and the mutant enzymes to this agent (Figure 6B). Based on the observation, that BAY 41-8543 lowered blood pressure in the Δ 3aa HET and WT rats, we tested whether the compound affects mutant PDE3A activity. sGC is expressed in HEK293 cells and inhibition of PDE3A through sGC activation and cGMP elevation induced by BAY 41-8543 changed the Δ FRET and thus caused inhibition of PDE3A (see above; Figure IE in the Supplement). Under resting conditions, enzyme activities of WT and mutant PDE3A2 variants were similar as there were no differences in emission intensities (Figure 6C).

We had demonstrated increased phosphorylation at S428 and S438 of mutant HTNB PDE3A enzymes in HeLa cells (T445N, T445S, T445A, A447T, A447V and G449V).⁴ We verified these results for the T445N variant using HEK293 cells, which do not express PDE3A endogenously. Figures 6D and E show that when expressed in HEK293 cells, PKC stimulation *via* phorbol-12-myristate-13-acetate (PMA) consistently increased the phosphorylation at S428 of the T445N and the Δ 3aa mutants compared to the WT. Forskolin stimulation caused a reduction of the phosphorylation at another serine, S312, for both mutants compared to the WT, most likely because PKA activates phosphatases.²⁴ Thus, there are consistently altered phosphorylation patterns for both mutants. In addition, mutant-specific alterations of the phosphorylation occur, which may account for the differences in activity between the mutants (Figures 6A-C).

Phosphorylation of S292/S293 by PKA recruits PDE3A1 into an A-kinase anchoring protein (AKAP)18-based signalosome at the sarcoplasmic reticulum of cardiac myocytes.¹⁶ To test whether *PDE3A* mutations that cause HTNB also alter protein-protein interactions, we expressed WT, the T445N and the Δ 3aa mutants in HEK293 cells and co-immunoprecipitated them with a known interaction partner of WT PDE3A, namely a scaffolding protein from the adaptor-protein family 14-3-3 (Figure 6F). The 14-3-3 proteins comprise a family of conserved regulatory molecules expressed in all eukaryotic cells. They can bind phosphorylated serine residues of a multitude of functionally diverse signaling proteins including kinases, phosphatases, and transmembrane receptors. An association between 14-3-3 θ and PMA-induced pS428 was described earlier.²⁵ Upon challenge with PMA, we observed an increase of pS428 (see above) and of the interactions of 14-3-3 θ with the mutants compared to the WT. Forskolin did not affect the interaction. The findings demonstrate that the HTNB phenotype is associated with altered phosphorylation and altered protein-protein interactions of PDE3A mutants.

Discussion

We present a new human *PDE3A* mutation that causes an amino acid substitution within a 5 amino acid-long *PDE3A* region N-terminally of the enzyme's catalytic domain. Diverse mutations in the encoding 15 bp gene segment are now known and only 3 bp to date are not *yet* involved. We introduce two new animal models, a hypertensive rat model that recapitulates the phenotypes of HTNB and a *PDE3A2* smooth muscle-specific overexpressing transgenic mouse model with hypertension. These animals underscore the role of increased peripheral vascular resistance as a driving mechanism for increasing blood pressure.

We suggest that our findings are relevant to essential hypertension as found in the general population. This point of view is supported by the robust linkage we found in a subfamily of Chinese subjects with essential hypertension that coincided with our *PDE3A* locus.²⁶ In addition, four independent genome-wide association studies (GWAS) identified the *PDE3A* locus and a fifth GWAS discusses its relevance.²⁷⁻³¹ Mendelian genetic evidence implicates sodium-(chloride) reabsorption in the distal nephron as responsible for hypertension.³² Previously, we tested the salt sensitivity of our HTNB subjects and determined that this form of hypertension is relatively salt resistant.²³ We measured serum electrolytes, sodium handling, and components of the renin-angiotensin-aldosterone axis in HTNB patient,²³ as well as in our rat and mouse models as reported here, and found no aberrancy compared to WT. We identified an increased VSMC proliferation rate, compromised vascular relaxation, and aberrant intracellular signaling suggesting such factors as contributors to hypertension, and as potential therapeutic targets.

Our data suggest that sGC activation could be suitable for the treatment of HTNB patients. The sGC stimulator BAY 41-8543 normalized the blood pressure in our $\Delta 3aa$ HET rat model. sGC activation causes elevation of cGMP and we showed that both BAY41-8543 and cGMP

could inhibit PDE3A. BAY 41-8543 and cGMP mediated the inhibition of the WT and the hyperactive T445N mutant enzymes when expressed in HeLa cells,^{4,33} our FRET experiments using HEK293 cells also point to an inhibitory effect of BAY 41-8543 on the hyperactive $\Delta 3aa$ PDE3A2 mutant. The inhibition is most likely due to the binding of cGMP to PDE3A and is probably operative in the rats. The apparently stronger inhibitory effect of BAY 41-8543 on the $\Delta 3aa$ mutant than on the WT is in line with the stronger blood pressure-lowering effect in the $\Delta 3aa$ HET rats than in the WT animals. However, the mechanism underlying the lowering of blood pressure in the rats may also involve the cGMP-mediated activation of PKG, which leads to vasodilation.³⁴

Compartmentalization of cAMP signaling in nano-domains is a common mechanism used by all cells to ensure the interaction of this second messenger within localized pools of appropriate effector proteins.³⁵ In this way, the cell can elicit differential responses by using a single, diffusible, molecular species.^{36,37} PDE enzymes are not haphazardly distributed but instead engage in protein-protein interactions, for example with AKAPs to establish cAMP signaling compartments.³⁸ In cardiac myocytes, PDE3A is part of an AKAP18-based signalosome consisting of PKA, phospholamban, and SERCA2a, which regulates Ca^{2+} reuptake into the SR and thereby relaxation of the heart.^{16,39} PDE3A is recruited into the complex upon PKA phosphorylation of S292/S293 and hydrolyzes the local cAMP establishing a negative feedback loop.¹⁶ Thus, the phosphorylation of PDE3A changes its localization.

We found that the S428 phosphorylation was consistently higher in the mutants than in WT, after activation of PKC, and we had previously shown that hyperactive PDE3A mutants that are aberrantly phosphorylated such as the T445N version are enriched in microsomal fractions when transiently expressed in HeLa cells.³³ We show here increased interactions of 14-3-3 θ to

the PDE3A mutants T445N and Δ 3aa. In analogy to the recruitment of PKA-phosphorylated PDE3A1, the increased phosphorylation-dependent interaction could change the localization of the mutants and, as a consequence, local cAMP would be reduced by the hyperactive enzymes. PKA phosphorylation of PDE3B promotes 14-3-3 θ binding and inhibits protein phosphatase-mediated inactivation.⁴⁰ Thus, binding of 14-3-3 θ may participate in the regulation of local activity of the mutant PDE3A versions at their cognate cellular location.

Collectively, the data in this study and our previous analysis of HTNB patients²³ indicate that PDE3A controls the blood pressure independent of the renin-angiotensin-aldosterone system and salt reabsorption by the kidney, but rather by influencing signaling in VSMC and their proliferation. Our findings suggest that by modulating PDE3A downstream signaling, in particular, its protein-protein interactions, new approaches to reduce blood pressure could be developed. Even the skeletal phenotype of HTNB patients might have therapeutic implications beyond cardiovascular medicine. Parathyroid hormone related peptide (PTHrP) is responsible for the brachydactyly we describe.⁴¹ This protein plays a role in the hypercalcemia of malignancy, and is involved in metastases of solid tumors.⁴² Our previous findings that PDE3A can regulate the PTHLH gene, which encodes PTHrP⁴, suggests that hypertension with brachydactyly may find use as a model for conditions unrelated to cardiovascular disease. Our vision is the development of precise intracellular pharmacological treatments that target PDE3A-directed nano-domains and thereby specifically influence intracellular signaling.

Acknowledgements

We thank our patients for their participation in these studies.

Author Contributions

FCL and EK designed the study and wrote the manuscript. MB, DNM, MN, and EP designed and supported generation of animal models. ME carried out FRET experiments and Western blotting. CS and ME carried out Western blotting and cell proliferation measurements. LM, SF, MT, and RP carried out and evaluated telemetric blood pressure measurements. SM, YC, DT, and MG measured and evaluated contractility parameters of isolated vessels. KeZ and AG measured cell proliferation of VSMC. HN and AH did microCT experiments. StS, MT and AH carried out echocardiography. FQ, TUPB and LM carried histological stainings and qPCRs. PGM, NG and NH were involved in genetic analysis. AM, BP, AA and RMI cloned. JE, ML and BW were involved in FRET experiments. MR carried out RIA. IK and RL supported animal studies. YMA discovered the novel German mutation. RH assisted in phenotyping in Turkey and conducted clinical protocols, in addition to chronicizing our events. SW recruited and phenotyped the German family with the G449S substitution. SB contributed to conceptualizing the study, genetic analyses and coordination of animal studies.

Sources of Funding

The Deutsche Forschungsgemeinschaft (DFG) supported the study to SB and EK (BÄ 1773/10-1, KL1415/7-1, and the program-project grant, 394046635 – SFB 1365), as well as by grants to EK from the Bundesministerium für Bildung und Forschung (BMBF; 16GW0179K), the German Centre for Cardiovascular Research (DZHK) partner site Berlin (81X2100146), and the German Israeli Foundation (GIF, I-1452-203/13-2018).

Disclosures

No author has a competing private or commercial interest.

Supplemental materials

German family with HTNB, substitution G449S

Expanded Methods

Overexpression of hyperactive PDE3A2 causes hypertension in mice

Supplemental Figures I-IV

Supplemental Tables I-III

Authors

Maria Ercu, MS^{1,2*}; Lajos Markó, MD, PhD^{2,3,4*}; Carolin Schächterle, PhD^{1,2,4};

Dmitry Tsvetkov, MD⁴; Yingqiu Cui, MD⁴; Sara Maghsodi, MS¹;

Theda U.P. Bartolomaeus, MS^{2,3,4}; Philipp G. Maass, PhD⁵; Kerstin Zühlke, PhD¹;

Nerine Gregersen, MD⁶; Norbert Hübner, MD^{1,2,3}; Russell Hodge, MA¹; Astrid Mühl, BS¹;

Bärbel Pohl, BS¹; Rosana Molé Illas, MD⁴; Andrea Geelhaar, BS¹; Stephan Walter, MD⁷;

Hanna Napieczynska, PhD¹; Stefanie Schelenz¹; Martin Taube¹; Arnd Heuser, MD¹;

Yoland-Marie Anistan, MD^{3,8}; Fatimunnisa Qadri, PhD¹; Mihail Todiras, MD¹;

Ralph Plehm, MS¹; Elena Popova, PhD¹; Reika Langanki, BS¹;

Jenny Eichhorst, Dipl.-Ing. (FH)⁹; Martin Lehmann, PhD⁹; Burkhard Wiesner, PhD⁹;

Michael Russwurm, MD¹⁰; Sofia K. Forslund, PhD^{1-4,11,13}; Ilona Kamer, BS⁴;

Dominik N. Müller, PhD^{1,2,4}; Maik Gollasch, MD, PhD^{4,8,12}; Atakan Aydin, PhD¹;

Sylvia Bähring, PhD⁴; Michael Bader, MD^{1,2,14}; Friedrich C. Luft, MD^{1,4, †};

Enno Klusmann, PhD^{1,2, †}

*ME and LM contributed equally to this project.

†FCL and EK are co-correspondents for this article.

¹Max-Delbrück-Center for Molecular Medicine (MDC) in the Helmholtz Association, Berlin, Germany; ²German Center for Cardiovascular Research (DZHK), Partner Site Berlin, Berlin, Germany; ³Charité-Universitätsmedizin Berlin, Berlin, Germany; ⁴Experimental and Clinical Research Center, a joint cooperation between the Charité Medical Faculty and the Max-Delbrück Center for Molecular Medicine, Berlin, Germany; ⁵Genetics and Genome Biology Program, Sickkids Research Institute and Department of Molecular Genetics, University of Toronto, Toronto ON, Canada; ⁶Auckland District Health Board (ADHB), Genetic Health Service New Zealand - Northern Hub, Auckland, New Zealand; ⁷Abteilung für Nephrologie/Hypertensiologie, St. Vincenz Krankenhaus, Limburg, Germany; ⁸Division of Nephrology and Intensive Care Medicine, Medical Department, Charité-Universitätsmedizin, Berlin, Germany; ⁹Leibniz-Forschungsinstitut für Molekulare Pharmakologie (FMP), Berlin, Germany; ¹⁰Institut für Pharmakologie und Toxikologie, Medizinische Fakultät MA N1, Ruhr-Universität Bochum, Bochum, Germany; ¹¹Berlin Institute of Health (BIH), Berlin, Germany; ¹²Department of Internal Medicine and Geriatrics, University Medicine Greifswald, Greifswald, Germany; ¹³European Molecular Biology Laboratory, Structural and Computational Biology Unit, Heidelberg, Germany; ¹⁴Institute for Biology, University of Lübeck, Lübeck, Germany

References

1. Olsen MH, Angell SY, Asma S, Boutouyrie P, Burger D, Chirinos JA, Damasceno A, Delles C, Gimenez-Roqueplo AP, Hering D, et al. A call to action and a lifecourse strategy to address the global burden of raised blood pressure on current and future generations: the Lancet Commission on hypertension. *Lancet*. 2016;388:2665-2712.
2. Seidel E and Scholl UI. Genetic mechanisms of human hypertension and their implications for blood pressure physiology. *Physiol Genomics*. 2017;49:630-652.
3. Schuster H, Wienker TE, Bähring S, Bilginturan N, Toka HR, Neitzel H, Jeschke E, Toka O, Gilbert D, Lowe A, et al. Severe autosomal dominant hypertension and brachydactyly in a unique Turkish kindred maps to human chromosome 12. *Nat Genet*. 1996;13:98-100.

4. Maass PG, Aydin A, Luft FC, Schachterle C, Weise A, Stricker S, Lindschau C, Vaegler M, Qadri F, Toka HR, et al. PDE3A mutations cause autosomal dominant hypertension with brachydactyly. *Nat Genet.* 2015;47:647-653.
5. van den Born BJ, Oskam LC, Zidane M, Schachterle C, Klussmann E, Bähring S and Luft FC. The Case| A handful of hypertension. *Kidney Int.* 2016;90:911-913.
6. Ercu M and Klussmann E. Roles of A-Kinase Anchoring Proteins and Phosphodiesterases in the Cardiovascular System. *J Cardiovasc Dev Dis.* 2018;5:14.
7. Choi YH, Ekholm D, Krall J, Ahmad F, Degerman E, Manganiello VC and Movsesian MA. Identification of a novel isoform of the cyclic-nucleotide phosphodiesterase PDE3A expressed in vascular smooth-muscle myocytes. *Biochem J.* 2001;353:41-50.
8. Popova E, Krivokharchenko A, Ganten D and Bader M. Efficiency of transgenic rat production is independent of transgene-construct and overnight embryo culture. *Theriogenology.* 2004;61:1441-1453.
9. Wilck N, Marko L, Balogh A, Kraker K, Herse F, Bartolomaeus H, Szijarto IA, Gollasch M, Reichhart N, Strauss O, et al. Nitric oxide-sensitive guanylyl cyclase stimulation improves experimental heart failure with preserved ejection fraction. *JCI Insight.* 2018;3:e96006.
10. Basu R, Poglitsch M, Yogasundaram H, Thomas J, Rowe BH and Oudit GY. Roles of Angiotensin Peptides and Recombinant Human ACE2 in Heart Failure. *J Am Coll Cardiol.* 2017;69:805-819.
11. Schleifenbaum J, Kassmann M, Szijártó IA, Hercule HC, Tano J-Y, Weinert S, Heidenreich M, Pathan AR, Anistan Y-M and Alenina N. Stretch-activation of angiotensin II type 1a receptors contributes to the myogenic response of mouse mesenteric and renal arteries. *Circ Res.* 2014;115:263-272.
12. Brooker G, Harper JF, Terasaki WL and Moylan RD. Radioimmunoassay of cyclic AMP and cyclic GMP. *Adv Cyclic Nucleotide Res.* 1979;10:1-33.
13. Chi J, Meng L, Pan S, Lin H, Zhai X, Liu L, Zhou C, Jiang C and Guo H. Primary Culture of Rat Aortic Vascular Smooth Muscle Cells: A New Method. *Med Sci Monit.* 2017;23:4014-4020.
14. DiPilato LM and Zhang J. The role of membrane microdomains in shaping beta2-adrenergic receptor-mediated cAMP dynamics. *Mol Biosyst.* 2009;5:832-837.
15. Vukicevic T, Hinze C, Baltzer S, Himmerkus N, Quintanova C, Zuhlke K, Compton F, Ahlborn R, Dema A, Eichhorst J, et al. Fluconazole Increases Osmotic Water Transport in Renal Collecting Duct through Effects on Aquaporin-2 Trafficking. *J Am Soc Nephrol.* 2019;30:795-810.
16. Ahmad F, Shen W, Vandeput F, Szabo-Fresnais N, Krall J, Degerman E, Goetz F, Klussmann E, Movsesian M and Manganiello V. Regulation of sarcoplasmic reticulum Ca²⁺-ATPase 2 (SERCA2) activity by phosphodiesterase 3A (PDE3A) in human myocardium: phosphorylation-dependent interaction of PDE3A1 with SERCA2. *J Biol Chem.* 2015;290:6763-6776.
17. Fan P, Zhang D, Yang KQ, Zhang QY, Luo F, Lou Y, Liu YX, Zhang HM, Song L, Cai J, Wu HY, et al. Hypertension and Brachydactyly Syndrome Associated With Vertebral Artery Malformation Caused by a PDE3A Missense Mutation. *Am J Hypertens.* 2020;33:190-197.
18. Boda H, Uchida H, Takaiso N, Ouchi Y, Fujita N, Kuno A, Hata T, Nagatani A, Funamoto Y, Miyata M, et al. A PDE3A mutation in familial hypertension and brachydactyly syndrome. *J Hum Genet.* 2016;61:701-703.

19. Renkema KY, Westermann JM, Nievelstein RAJ, Lo ANSM, van der Zwaag B, Manshande ME and van Haelst MM. PDE3A gene screening improves diagnostics for patients with Bilginturan syndrome (hypertension and brachydactyly syndrome). *Hypertens Res.* 2018;41:981-988.
20. Naraghi R, Schuster H, Toka HR, Bahring S, Toka O, Oztekin O, Bilginturan N, Knoblauch H, Wienker TF, Busjahn A, et al. Neurovascular compression at the ventrolateral medulla in autosomal dominant hypertension and brachydactyly. *Stroke.* 1997;28:1749-1754.
21. Begum N, Hockman S and Manganiello VC. Phosphodiesterase 3A (PDE3A) deletion suppresses proliferation of cultured murine vascular smooth muscle cells (VSMCs) via inhibition of mitogen-activated protein kinase (MAPK) signaling and alterations in critical cell cycle regulatory proteins. *J Biol Chem.* 2011;286:26238-26249.
22. Movsesian M. Novel approaches to targeting PDE3 in cardiovascular disease. *Pharmacol therapeut.* 2016;163:74-81.
23. Schuster H, Wienker TF, Toka HR, Bahring S, Jeschke E, Toka O, Busjahn A, Hempel A, Tahlhammer C, Oelkers W, et al. Autosomal dominant hypertension and brachydactyly in a Turkish kindred resembles essential hypertension. *Hypertension.* 1996;28:1085-1092.
24. Zolnierowicz S. Type 2A protein phosphatase, the complex regulator of numerous signaling pathways. *Biochem Pharmacol.* 2000;60:1225-1235.
25. Pozuelo Rubio M, Campbell DG, Morrice NA and Mackintosh C. Phosphodiesterase 3A binds to 14-3-3 proteins in response to PMA-induced phosphorylation of Ser428. *Biochem J.* 2005;392:163-172.
26. Gong M, Zhang H, Schulz H, Lee YA, Sun K, Bahring S, Luft FC, Nurnberg P, Reis A, Rohde K, et al. Genome-wide linkage reveals a locus for human essential (primary) hypertension on chromosome 12p. *Hum Mol Genet.* 2003;12:1273-1277.
27. Ehret GB, Ferreira T, Chasman DI, Jackson AU, Schmidt EM, Johnson T, Thorleifsson G, Luan J, Donnelly LA, Kanoni S, et al. The genetics of blood pressure regulation and its target organs from association studies in 342,415 individuals. *Nat Genet.* 2016;48: 1171-1184.
28. Kato N, Loh M, Takeuchi F, Verweij N, Wang X, Zhang W, Kelly TN, Saleheen D, Lehne B, Mateo Leach I, et al. Trans-ancestry genome-wide association study identifies 12 genetic loci influencing blood pressure and implicates a role for DNA methylation. *Nat Genet.* 2015;47:1282-1293.
29. Simino J, Sung YJ, Kume R, Schwander K and Rao DC. Gene-alcohol interactions identify several novel blood pressure loci including a promising locus near SLC16A9. *Frontiers in genetics.* 2013;4:277.
30. Warren HR, Evangelou E, Cabrera CP, Gao H, Ren M, Mifsud B, Ntalla I, Surendran P, Liu C, Cook JP, et al. Genome-wide association analysis identifies novel blood pressure loci and offers biological insights into cardiovascular risk. *Nat Genet.* 2017;49:403-415.
31. Evangelou E, Warren HR, Mosen-Ansorena D, Mifsud B, Pazoki R, Gao H, Ntritsos G, Dimou N, Cabrera CP, Karaman I, et al. Genetic analysis of over 1 million people identifies 535 new loci associated with blood pressure traits. *Nat Genet.* 2018;50:1412-1425.
32. Lifton RP, Gharavi AG and Geller DS. Molecular mechanisms of human hypertension. *Cell.* 2001;104:545-556.
33. Toka O, Tank J, Schachterle C, Aydin A, Maass PG, Elitok S, Bartels-Klein E, Hollfinger I, Lindschau C, Mai K, et al. Clinical Effects of Phosphodiesterase 3A Mutations in Inherited Hypertension With Brachydactyly. *Hypertension.* 2015;66:800-808.

34. Hofmann F, Bernhard D, Lukowski R and Weinmeister P. cGMP regulated protein kinases (cGK). *Handb Exp Pharmacol*. 2009;137-162.
35. Musheshe N, Schmidt M and Zaccolo M. cAMP: From Long-Range Second Messenger to Nanodomain Signalling. *Trends Pharmacol Sci*. 2018;39:209-222.
36. McCormick K and Baillie GS. Compartmentalisation of second messenger signalling pathways. *Curr Opin Genet Dev*. 2014;27:20-25.
37. Dema A, Perets E, Schulz MS, Deak VA and Klussmann E. Pharmacological targeting of AKAP-directed compartmentalized cAMP signalling. *Cell Signal*. 2015;27:2474-2487.
38. Klussmann E. Protein-protein interactions of PDE4 family members - Functions, interactions and therapeutic value. *Cell Signal*. 2016;28:713-718.
39. Lygren B, Carlson CR, Santamaria K, Lissandron V, McSorley T, Litzenberg J, Lorenz D, Wiesner B, Rosenthal W, Zaccolo M, Tasken K and Klussmann E. AKAP complex regulates Ca²⁺ re-uptake into heart sarcoplasmic reticulum. *EMBO Rep*. 2007;8:1061-1067.
40. Palmer D, Jimmo SL, Raymond DR, Wilson LS, Carter RL and Maurice DH. Protein kinase A phosphorylation of human phosphodiesterase 3B promotes 14-3-3 protein binding and inhibits phosphatase-catalyzed inactivation. *J Biol Chem*. 2007;282:9411-9419.
41. Maass PG, Wirth J, Aydin A, Rump A, Stricker S, Tinschert S, Otero M, Tsuchimochi K, Goldring MB, Luft FC, et al. A cis-regulatory site downregulates PTHLH in translocation t(8;12)(q13;p11.2) and leads to Brachydactyly Type E. *Hum Mol Genet*. 2010;19:848-860.
42. Roodman GD. Genes associate with abnormal bone cell activity in bone metastasis. *Cancer Metastasis Rev*. 2012;31:569-578.

Table 1.

Serum or plasma parameters	WT	Δ3aa HET	functional DEL
Sodium (mmol/L)	141.68 \pm 1.57	140.88 \pm 0.90	141.14 \pm 1.8
Potassium (mmol/L)	5.97 \pm 0.24	5.33 \pm 0.59	4.76 \pm 0.42
Chloride (mmol/L)	101.74 \pm 0.46	102.40 \pm 1.67	100.68 \pm 2.13
Urea nitrogen (mg/dL)	35.42 \pm 3.99	39.40 \pm 3.86	33.34 \pm 0.37
Creatinine (mg/dL)	0.35 \pm 0.04	0.32 \pm 0.02	0.38 \pm 0.06
Cystatin (mg/L)	0.23 \pm 0.04	0.23 \pm 0.02	0.21 \pm 0.03
Angiotensinogen (μ g/ml)	22.07 \pm 2.73	21.56 \pm 3.51	21.40 \pm 1.52
Renin (ng/AngI/ml/h)	6.14 \pm 6.04	2.37 \pm 1.44	9.43 \pm 10.63
Urine parameters			
Sodium (mmol/L)	57.95 \pm 30.88	54.22 \pm 28.17	96.11 \pm 39.79
Potassium (mmol/L)	88.74 \pm 46.75	106.63 \pm 24.55	109.58 \pm 21.70
Chloride (mmol/L)	78.52 \pm 33.83	78.74 \pm 15.96	125.14 \pm 29.41 #(p = 0.03)
Urea nitrogen (mg/dL)	1621.70 \pm 650.72	1732.11 \pm 195.83	1859.35 \pm 423.59
Creatinine (mg/dL)	34.60 \pm 15.59	32.38 \pm 5.07	34.10 \pm 7.49
Albumin (mg/dL)	0.13 \pm 0.10	0.15 \pm 0.12	0.51 \pm 0.36
Calculated parameters			
FENa (%)	0.46 \pm 0.21	0.37 \pm 0.15	0.75 \pm 0.25 *(p = 0.03)
FEK (%)	18.04 \pm 5.72	19.95 \pm 5.40	25.94 \pm 5.11
FECl (%)	0.79 \pm 0.06	0.75 \pm 0.05	1.38 \pm 0.20 #(p < 0.001)
Urine/ albumin creatinine (mg/mmol)	0.49 \pm 0.54	0.58 \pm 0.49	1.60 \pm 0.85

Table 1. Plasma and urine parameters determined of wild-type (WT), heterozygous (Δ 3aa HET), and functional deletions (DEL) rats. Shown are plasma, urine and calculated values. Statistical comparison was carried out by one-way analysis of variance. n = 4-5 animals per group, *p<0.05 vs. Δ 3aa HET and #p<0.05 vs. WT and Δ 3aa HET, Tukey's post-hoc test. Values are means \pm SD. FE, fractional excretion

Figure Legends

Figure 1. HTNB mutations are located in a 15 bp region of the *PDE3A* gene. All the HTNB mutations known to date are shown. A conserved 15 bp regulatory hot spot region is invariably affected. The mutations in the 15 bp regulatory region alter the isoforms PDE3A1 and PDE3A2.

Figure 2. A rat model of HTNB. A rat model harboring a 9 bp (3 amino acid) deletion ($\Delta 3aa$) within the hotspot depicted in Figure 1 was generated with CRISPR/Cas9. A second model features a 20 bp deletion ($\Delta 20$ bp) that results in a frameshift and thus in a truncated and functionally deleted protein (functional DEL). Sequences of human, mouse and rat *PDE3A* genes and proteins are aligned.

Figure 3. A G449S substitution in *PDE3A* is associated with HTNB. A novel amino acid substitution, G449S, encoded in the mutational hotspot region of the *PDE3A* gene was identified (see also Figure 1). Shown are photographs and roentgenograms of the mother's hands and feet (age 54 years; I/2). The hypertension and skeletal phenotypes are similar as those earlier described.⁴

Figure 4. A rat model expressing mutant *PDE3A* recapitulates HTNB. A. Detection of PDE3A1 and PDE3A2 in aorta of WT, $\Delta 3aa$ HET and the rat model without expression of *PDE3A* (functional DEL) by Western blotting. The expression of the *PDE3A* isoforms was not detectable in the functional DEL animals. Lower panel, semiquantitative analysis of the expression of the two isoforms by densitometry of the signals. n = 4 independent experiments; data are

mean \pm SEM, *** $p < 0.001$, **** $p < 0.0001$. **B.** The affected $\Delta 3aa$ HET rats had shorter forepaw metacarpal bones III than WT and the functionally deleted (functional DEL) PDE3A rats (WT = 4, $\Delta 3aa$ HET = 7, PDE3A functionally deleted = 5). The images were obtained by microCT measurements of the left forepaw. Quantitation is from the metacarpal bone III; data are mean \pm SEM, ** $p < 0.01$, **** $p < 0.0001$. **C.** Heterozygous $\Delta 3aa$ (red), homozygous $\Delta 3aa$ (blue), WT (black), PDE3A functionally deleted (DEL; green) rats were monitored for >10 days with radio-telemetry. The plots show blood pressure (systolic/diastolic mmHg) as well as heart rate (beats per minute; BPM) over time (horizontal axis, night phases marked in black). Curves show *loess* fits made using R package ggplot2 with gray intervals indicating 95 % confidence intervals for *loess* parameters. Horizontal lines represent model expectation value for WT and the mutant rats. Lower black bars depict night periods. The systolic blood pressure between all groups is significantly different. Only the systolic blood pressures of $\Delta 3aa$ HET and HOM rats were not significantly different. The diastolic blood pressure differs significantly between all groups. The heart rate is only significantly different between the functional DEL and $\Delta 3aa$ HET and the functional Del and the $\Delta 3aa$ HOM. All p values are listed in Table II in the Supplement. Significance (nested model likelihood ratio test p value) and effect size (model fit parameter, same unit as vertical axis) is noted. **D.** Cardiac output of WT, heterozygous $\Delta 3aa$ (HET) and homozygous $\Delta 3aa$ (HOM) PDE3A rats was estimated by echocardiography. Cardiac output was measured by tracing the endocardium in systole and diastole of a parasternal long axis view of the left ventricle. The differences were statistically not significant. **E.** Heterozygous $\Delta 3aa$ (HET) PDE3A rats show loops in the posterior inferior cerebellar arteries (PICA). Brain vessels were perfused with Microfil and visualized using microCT. Shown are representative images from $n = 2$ $\Delta 3aa$ HET

and $n = 5$ WT rats. **F.** Myograph experiments using aortic rings document that the $\Delta 3aa$ heterozygous (HET) rats have lower relaxation capacity in response to forskolin (adenylate cyclase stimulator) than WT aortic rings and rings from the PDE3A functionally deleted (DEL) rats (WT, $n = 3$; $\Delta 3aa$ heterozygous, $n = 4$; PDE3A functional DEL, $n = 4$); data are mean \pm SEM, $*p < 0.05$, $**p < 0.01$. **G.** The media to lumen ratio of second-order mesenteric arteries in $\Delta 3aa$ heterozygous (HET) rats is increased compared to WT animals. Presented are representative images from 3-5 mesenteric arteries per rat. $n = 3$ WT, $n = 3$ $\Delta 3aa$ HET and $n = 2$ functional DEL rats. The quantification shows means \pm SEM. $**p < 0.01$ ***, $p < 0.001$. **H.** The concentration of cAMP in resting second-order mesenteric arteries is lower in $\Delta 3aa$ heterozygous (HET) rats than in WT animals. The cAMP levels were determined by radioimmuno assay (RIA). Second-order mesenteric arteries were obtained from 2 animals per group; cAMP was measured in $n = 4$ arteries from WT and $n = 3$ arteries from $\Delta 3aa$ heterozygous (HET) rats, mean \pm SEM, $*p < 0.05$. **I.** The myogenic tone of rat third-order mesenteric arteries from WT and $\Delta 3aa$ heterozygous (HET) rats was determined. Upper panels, diameter of mesenteric arteries recorded during pressure steps incrementally elevated from 20 to 100 mmHg. Vessels were incubated in physiological salt solution (PSS, $+Ca^{2+}$) or Ca^{2+} -free PSS ($-Ca^{2+}$). Lower left panel, Myogenic tone expressed as dilation of vessels induced by Ca^{2+} -free PSS. Lower middle and right panels, pressurized (100 mmHg) mesenteric arteries ($n = 4$ vessels from 4 rats) from $\Delta 3aa$ HET showed weaker dilation in response to forskolin than vessels from WT rats ($n = 3$ from 3 rats). Dotted line shows the diameter of a wild-type vessel (320 μm) and of a $\Delta 3aa$ HET vessel (500 μm). $p < 0.05$, n.s., not significant. **J.** Primary VSMC derived from aorta of $\Delta 3aa$ heterozygous (HET) rats proliferate faster than those from WT and PDE3A functionally deleted (DEL) rats. VSMC from $n = 6$ animals per group were counted every 24 h. Shown are mean \pm SEM, $*p < 0.05$. **K.** WT and $\Delta 3aa$

heterozygous (HET) rats were submitted to blood-pressure lowering treatments and found that a single gavage dose (3 mg/kg) of the sGC stimulator BAY 41-8543 lowered the mean arterial pressure (MAP) within 3 h in $\Delta 3aa$ HET to a similar level as in WT rats; $n = 5$ WT and 4 $\Delta 3aa$ HET rats; mean \pm SEM, * $p < 0.05$, ** $p < 0.01$.

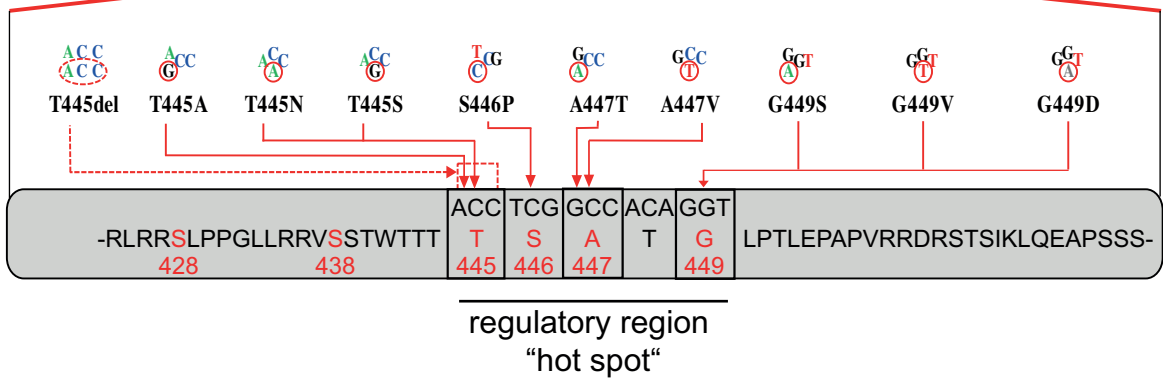
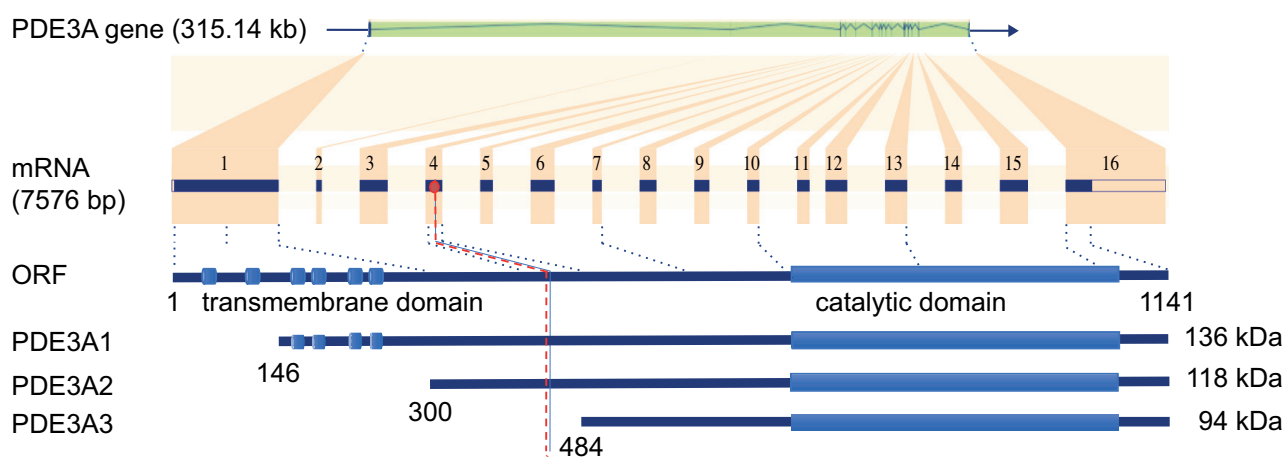
Figure 5. Schematic representation of the renin-angiotensin-aldosterone system in wild-type and mutant rats. The indicated parameters of the renin-angiotensin-aldosterone system were investigated in wild-type (WT), heterozygous $\Delta 3aa$ (HET) and PDE3A functionally deleted (DEL) rats. Similar sizes of spheres indicate similar relative concentrations (all in pmol/L). $n = 5$ animals per group. Values are means \pm SD. n.d., not determinable; n.a., not available.

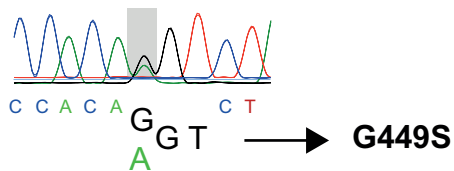
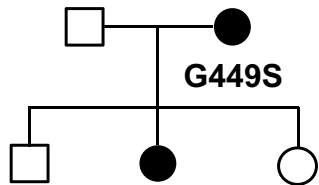
Figure 6. Activity, phosphorylation, and interactions of PDE3A2 mutants are different.

A. FRET to determine PDE3A activity in a single-cell approach. Upper panels: The FRET sensor (ICUE3; cyan and yellow) and the indicated PDE3A2 variants (red) co-localize (orange) in HEK293 cells when co-expressed. Scale bar, 20 μm . Lower left panel: Western blotting with an anti-PDE3A antibody demonstrated that the PDE3A2-mCherry variants were similarly expressed in HEK293 cells, which lack endogenous expression of PDE3A. The sensor was detected with an anti-GFP antibody. GAPDH served as the loading control. Lower right panel: Shown is the Δ FRET. 0 reflects the basal cAMP levels. Increases in Δ FRET indicate higher cAMP levels, consistent with decreased PDE3A activity. Forskolin stimulates adenylate cyclase, while milrinone inhibits PDE3A. Upon forskolin stimulation, the T445N mutant, the $\Delta 3aa$ deletion and the G449S mutation revealed significantly increased PDE3A activity, indicated by the negative Δ FRET values, which in turn indicate lower cAMP levels in those conditions as compared to the

WT. When the effect of forskolin alone (30 μ M) was examined, the substance was added and the measurement immediately started. When the effect of milrinone was investigated, the cells were incubated with the agent (30 μ M) for 30 min *prior* to the addition of forskolin (30 μ M) and subsequent measurement. Statistical analysis was carried out using two-way ANOVA and Bonferroni multi-comparison, $n \geq 4$ independent experiments and analysis of 24-65 individual cells per PDE3A2 variant and condition. Shown are mean \pm SEM, ** $p < 0.01$; *** $p < 0.001$. Further controls including measurements of independent CFP and Venus, non-interacting co-expressed CFP and Venus or of a CFP-YFP tandem construct are shown in Figures IIIB and IIIC in the Supplement. **B.** The PDE3A inhibitor cilostamide (10 μ M) inhibits WT and the indicated PDE3A2 mutant versions to a similar extent. Cilostamide (10 μ M) and forskolin (30 μ M) were added simultaneously and the measurement immediately started. $n = 3$ independent experiments per PDE3A2 version. **C.** Under resting conditions, the cAMP hydrolytic activity of WT and the indicated PDE3A2 mutants is similar as indicated by the similar emission intensities. **D.** To compare the effect of forskolin and the PKC stimulator, phorbol-12-myristate-13-acetate (PMA), on the phosphorylation of S312, S428 and S438 of the WT, the T445N mutant and the rat PDE3A2- Δ 3aa deletion, these proteins were expressed in HEK293 cells. The cells were stimulated with the agents and phosphorylation was detected by Western blotting with phosphate site-specific antibodies. Representative blots from $n=3$ independent experiments is shown. **E.** The semi-quantitative analysis of Western blots from Figure 7D by densitometry. Ordinate shows ratios of signals for mutant relative to control WT PDE3A2. Upon PMA stimulation, the S428 phosphorylation consistently increased in both mutants compared to WT. Forskolin stimulation consistently decreased S312 phosphorylation of the mutants compared to WT. $n = 3$; shown are mean \pm SEM, *** $p < 0.001$. **F.** The stimulation with PMA increased the interaction of the mutant T445N and the Δ 3aa

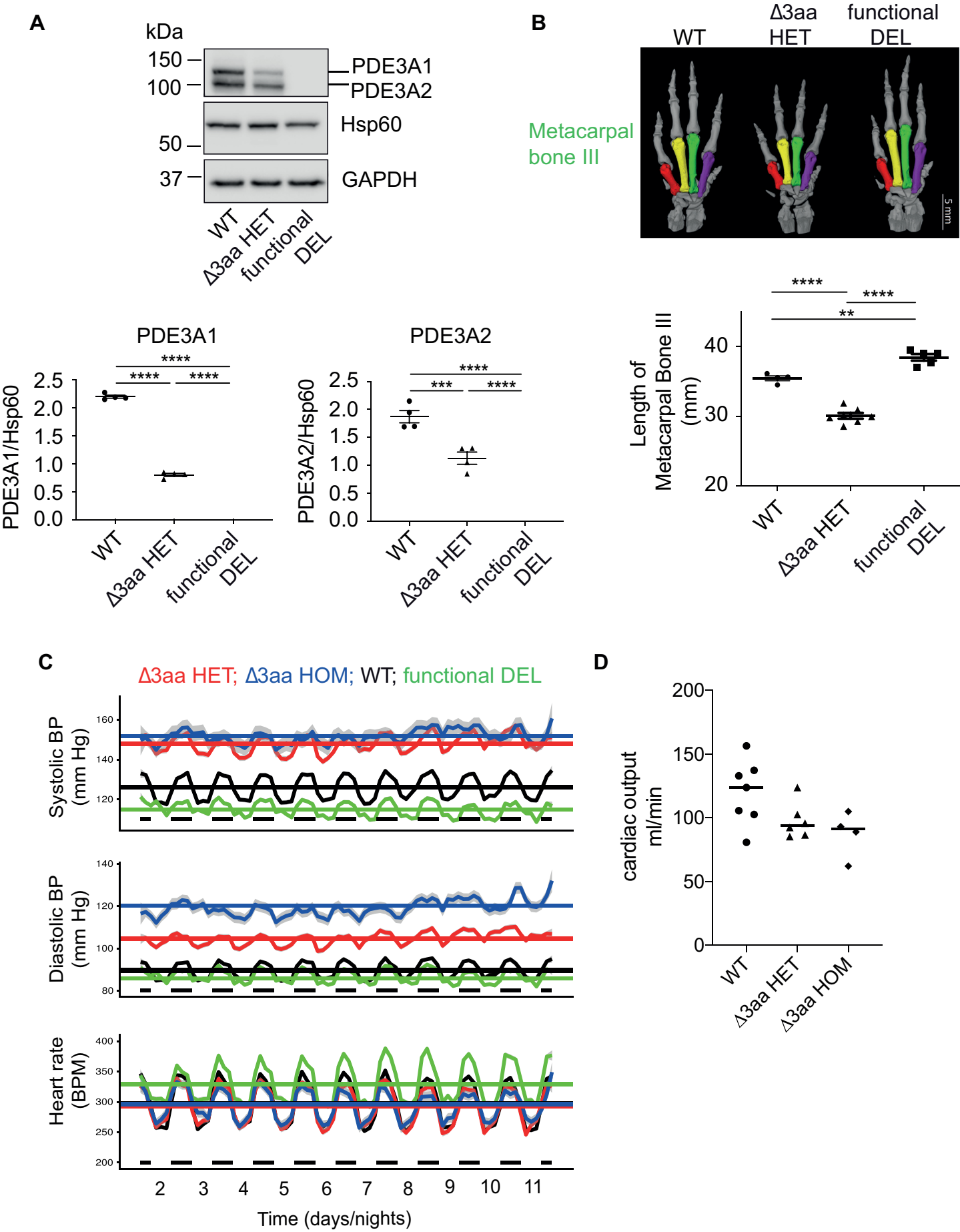
deletion with the adapter protein, 14-3-3 θ , compared to WT. WT and the PDE3A2 mutants T445N and PDE3A2- Δ 3aa were transiently expressed in HEK293 cells and immunoprecipitated *via* their Flag tags. Similar precipitation efficiencies were confirmed by detection of PDE3A2 with an anti-Flag tag antibody by Western blotting. Co-immunoprecipitated 14-3-3 θ was also detected by Western blotting. Relative interaction of 14-3-3 θ with the mutant PDE3A2 versions compared to control PDE3A2-WT-Flag is shown. Semiquantitative analysis was carried out by densitometry. n = 6, shown are mean \pm SEM, ***p < 0.001.

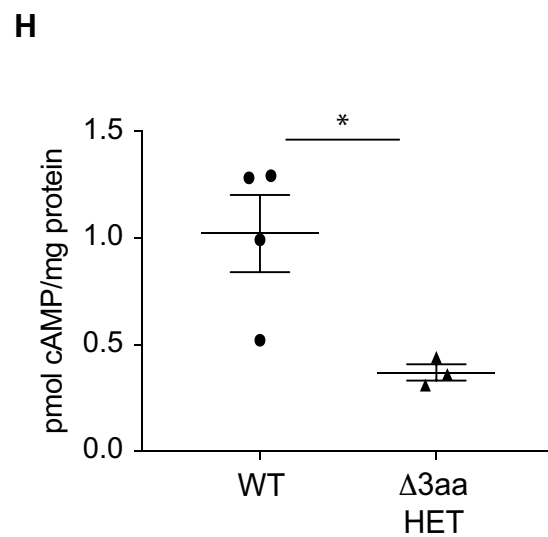
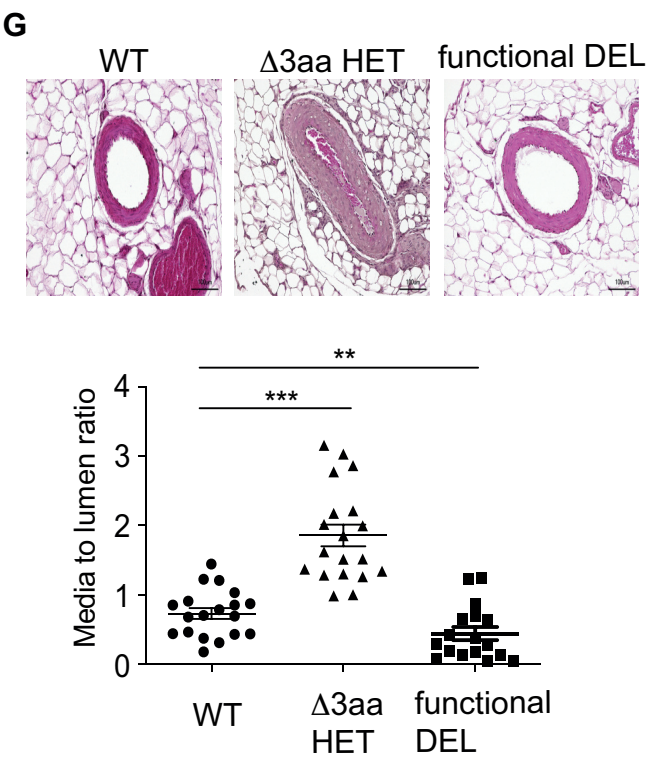
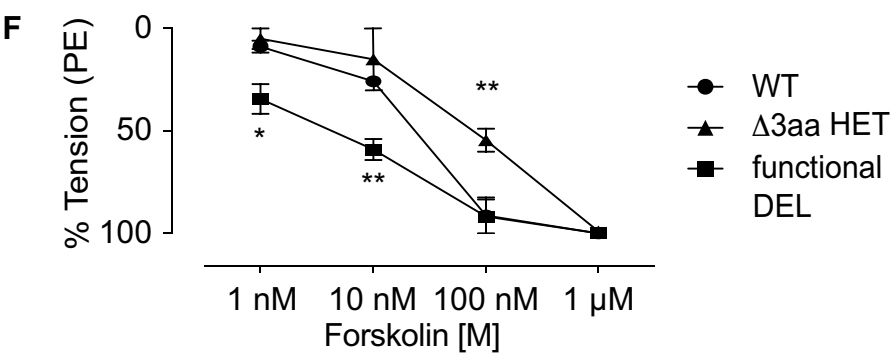
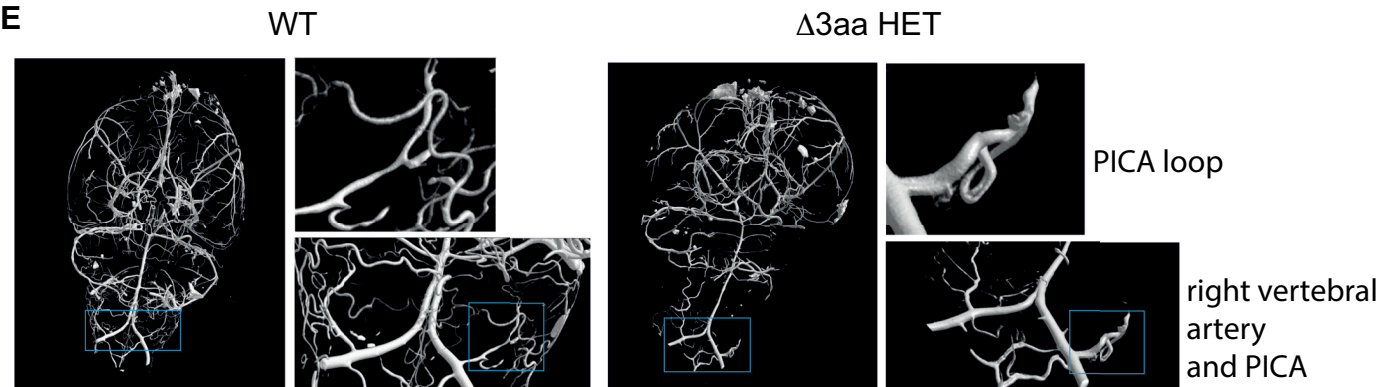




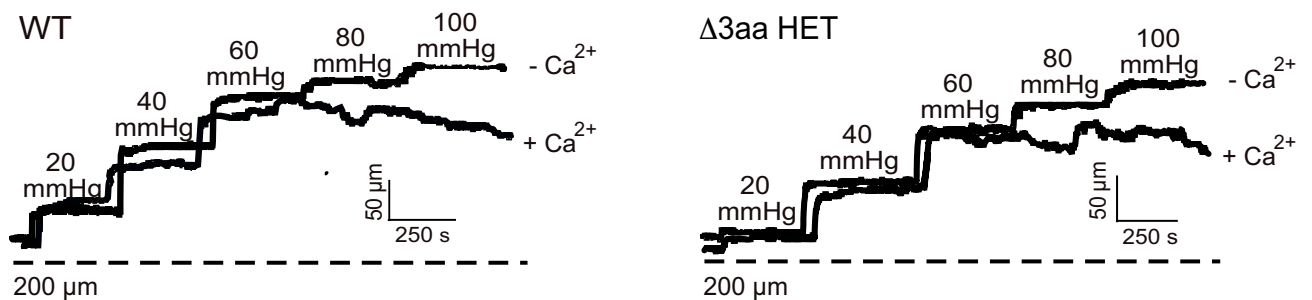
I/2

II/2

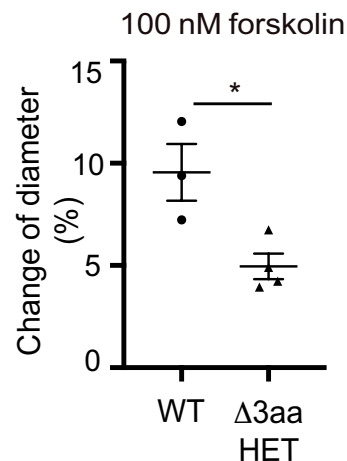
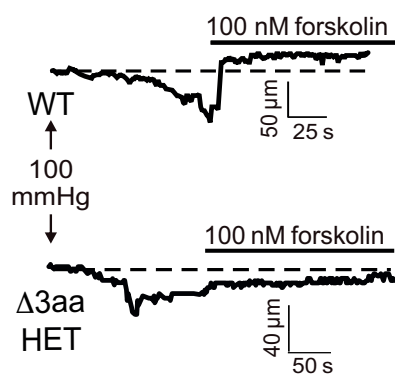
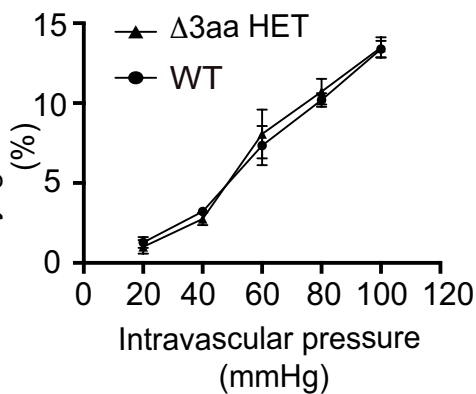




I

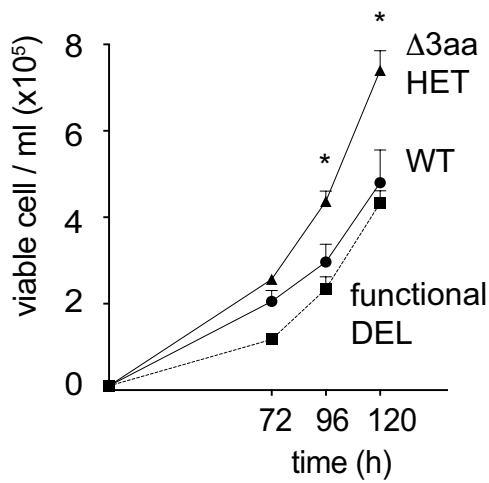


Myogenic tone (%)

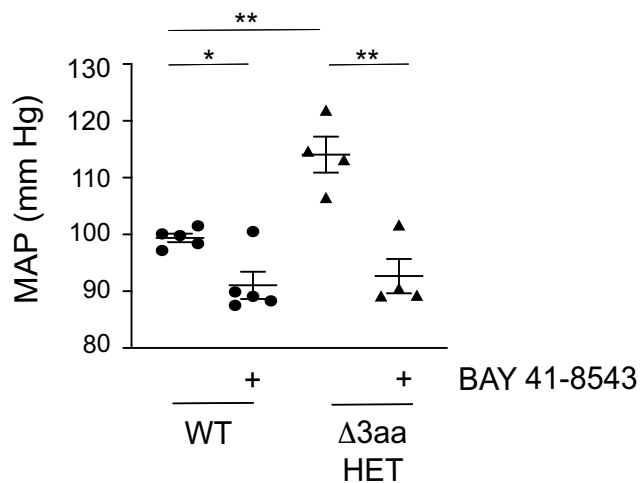


J

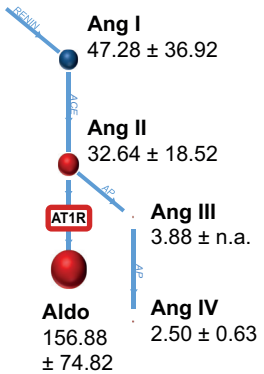
Primary vascular smooth muscle cells



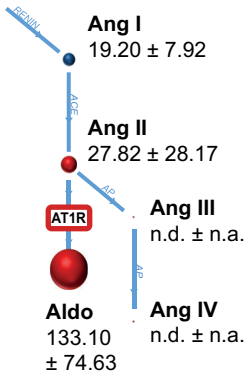
K



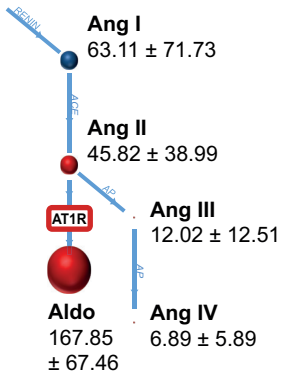
WT

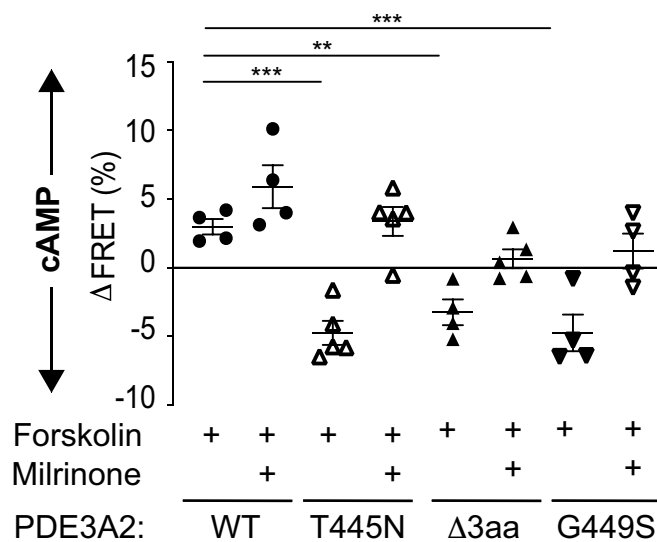
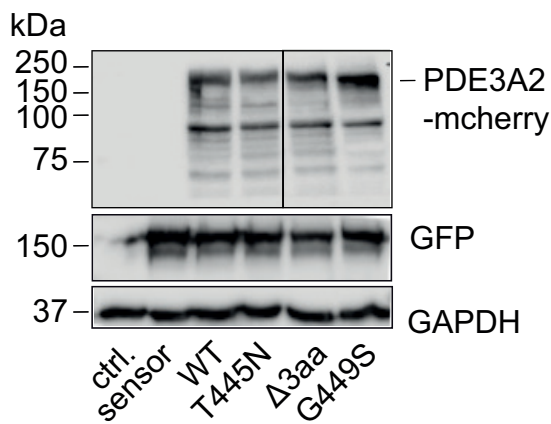
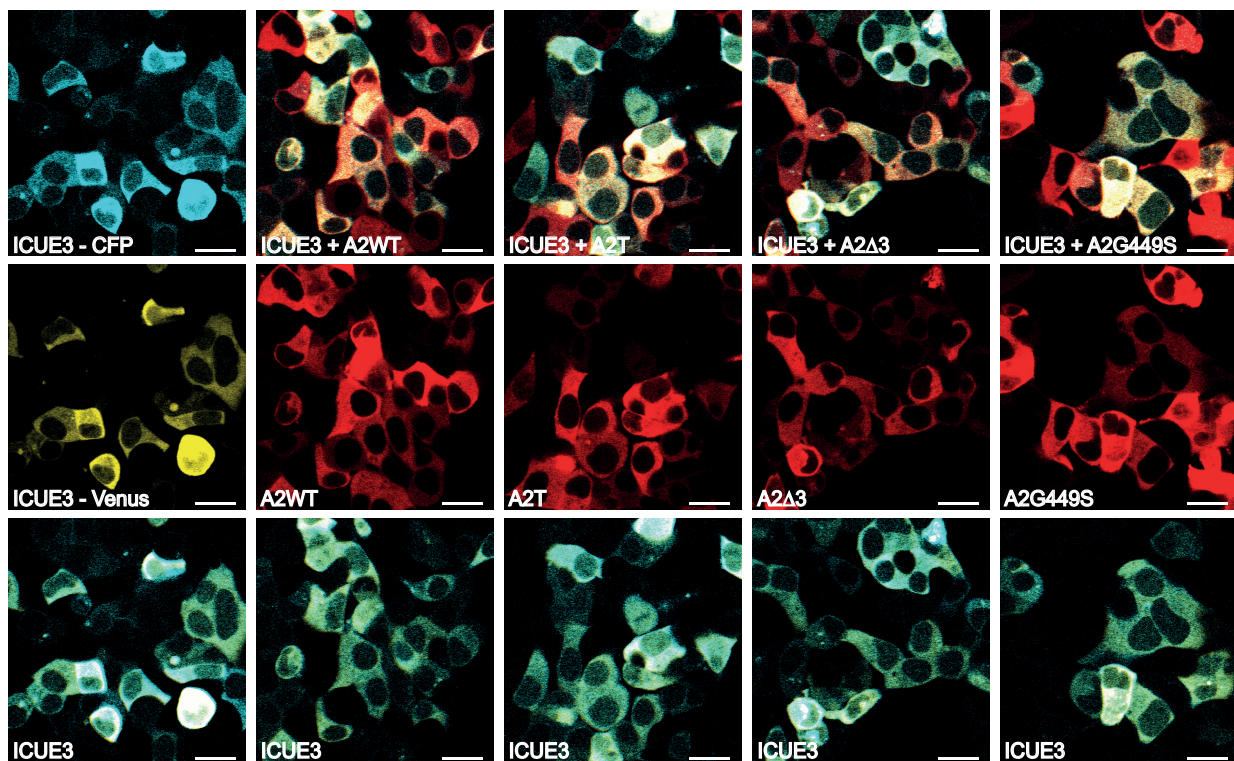
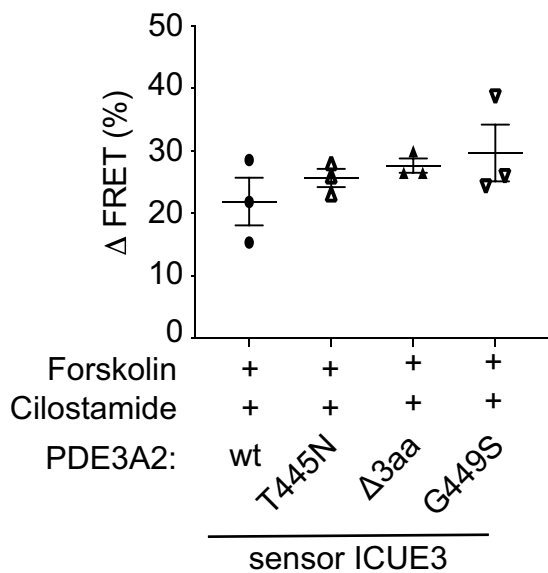
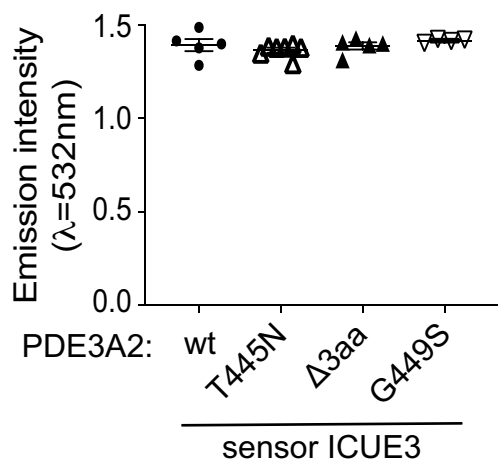


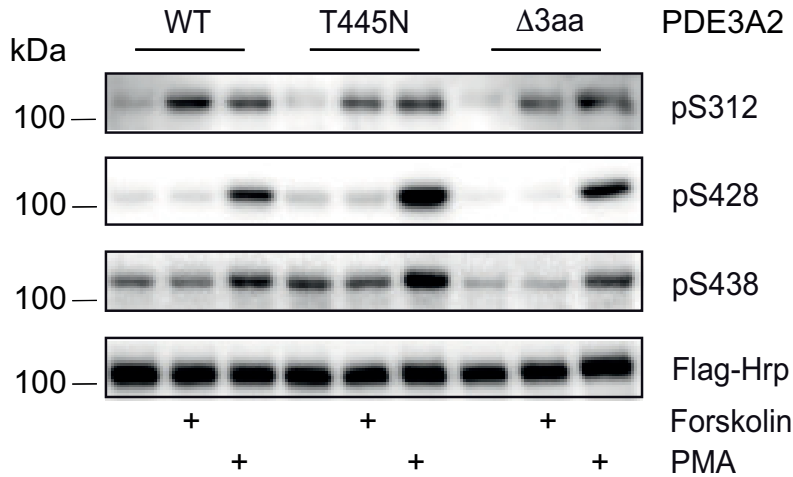
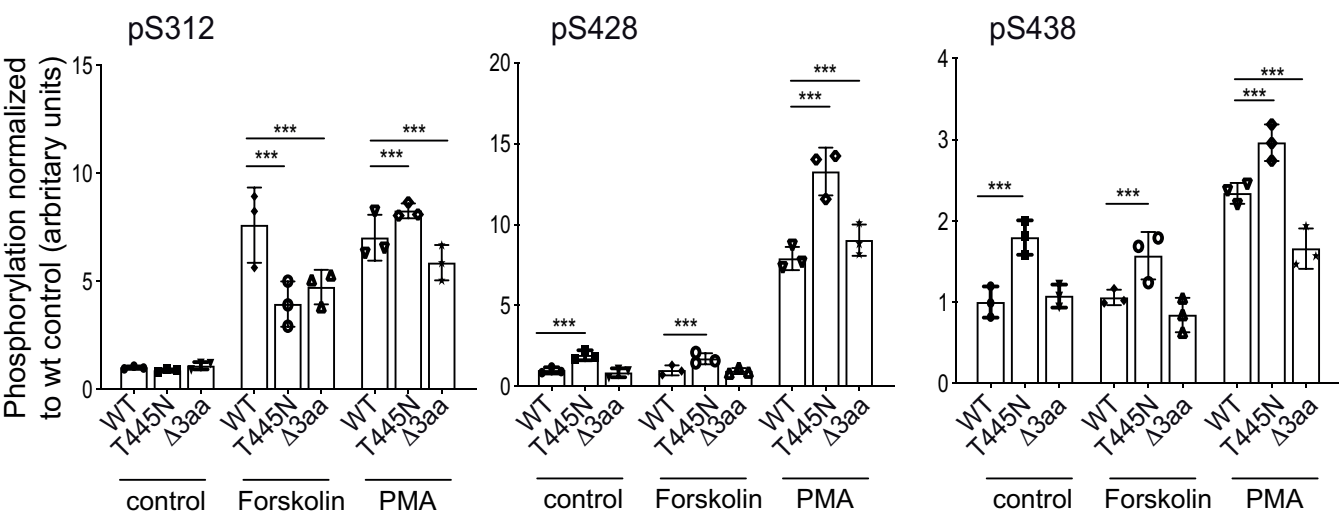
$\Delta 3\text{aa}$ HET



functional
DEL



A**B****C**

D**E****F**